EPJ Web of Conferences **274**, 07013 (2022) https://doi.org/10.1051/epjconf/202227407013
XVth Quark Confinement and the Hadron Spectrum

Is there pasta in neutron stars?

Nicolas Chamel[1,*], *John Michael* Pearson[2], and *Nikolai* Shchechilin[1]

[1]Institute of Astronomy and Astrophysics, Université Libre de Bruxelles, CP 226, Boulevard du Triomphe, B-1050 Brussels, Belgium
[2]Dépt. de Physique, Université de Montréal, Montréal (Québec), H3C 3J7 Canada

Abstract. The interior of neutron stars may contain a mantle made of very exotic neutron-proton clusters with unusual shapes such as rods or slabs collectively referred to as "nuclear pastas" coexisting with free nucleons and a charge neutralizing gas of electrons. Adding shell and pairing effects perturbatively and consistently to the fourth-order extended Thomas-Fermi method using the Brussels-Montreal functional BSk24, we find that nuclear pastas are much less abundant than previously thought from liquid-drop models, thus questioning their very existence in neutron stars.

1 Introduction

Neutron stars are the extremely compact remnants of gravitational core-collapse supernova explosions. Initially very hot, they rapidly cool down by emitting neutrinos and later photons, as monitored over more than a decade in the Cassiopeia A remnant [1]. Neutron stars contain matter that is so cold and dense that it cannot be created in the laboratory (see, e.g., Ref. [2] for a recent review). According to our current understanding, a neutron star is stratified into distinct layers. Below a thin atmosphere (a Coulomb plasma of electrons and light elements), the surface is probably covered by an iron-rich metallic ocean. Due to the prodigious gravitational pressure in the floor and the solid layers beneath, atoms are ionized and thus coexist with a quantum gas of free electrons. With increasing depth, matter becomes progressively more neutron rich until unbound neutrons appear. The inner region of the crust is therefore permeated by a neutron ocean. At about half the density found inside heavy nuclei, the crust dissolves into a homogeneous liquid mixture of nucleons and electrons.

In the outer crust, nuclei remain sufficiently far apart that their structure is not influenced by their neighbors and is essentially governed by the short-range nuclear and Coulomb interactions. Nuclei are therefore expected to have a quasi-spherical shape, as in vacuum. The long-range Coulomb interactions between nuclei come into play only for determining their global spatial arrangement; nuclei are expected to crystallize in a body-centered cubic lattice (see, e.g., Ref. [3] and references therein). However, these interactions become increasingly important in deeper regions. In the densest part of the crust, matter is so compressed that the spacing between nuclei becomes comparable to their size. Back in 1971, Baym, Bethe and Pethick [4] showed within a compressible liquid-drop treatment that the equilibrium shape of nuclei is determined by the balance between surface and Coulomb forces. They found that the filling fraction of nuclei u increases monotonically with density and anticipated that nuclear

*e-mail: nicolas.chamel@ulb.be

deformations could become important. They speculated that nuclei "turn inside out" as u exceeds 50%. Detailed calculations later showed that clusters with very peculiar shapes collectively referred to as "nuclear pasta" could form [5]. Quite generically, the liquid-drop approach [6, 7] predicts that spherical nuclei are no longer energetically favored above $u \sim 0.2$ (see also Refs. [8, 9] and references therein). Beyond this point, different types of structures are expected to appear independently of the adopted nuclear parametrization [7]: cylinders ("spaghetti") for $u \lesssim 0.35$, slabs ("lasagna") for $u \lesssim 0.65$, inverted cylinders ("buccatini") for $u \lesssim 0.8$ and bubbles ("Swiss cheese") for higher filling fractions. Following this culinary terminology, the phase with spherical clusters is sometimes referred to as "polpete" or "gnocchi". Later, calculations showed that nuclear pastas could account for half of the mass of the neutron-star crusts [10], and this has been supported by recent studies [11, 12]. However, these conclusions may change depending on how the liquid-drop model is implemented. In particular, the equilibrium shape turns out to be very sensitive to the surface terms and to the way they are described when corrections due to curvature and neutron skin are considered. For instance, pastas are present when one or the other correction is included [11, 13, 14] but not both [15, 16] while using the same nuclear parametrization for the bulk part of the energy, namely SLy4 [17]. The contributions of surface effects to the energy remain a thorny issue. They are not determined by the liquid-drop model itself but must be either parametrized empirically or inferred from a more microscopic treatment of dense inhomogeneous matter.

By considering the local distributions of nucleons, the Thomas Fermi theory provides a better description of nuclear clusters. In this way, nucleons that are free and those bound inside clusters are treated consistently. Moreover, the diffuseness of the clusters is taken into account, thus ensuring a more accurate evaluation of the energy contributions related to surface effects. These improvements lead to different predictions for pasta phases, as shown, e.g., in Ref. [18]. Further developments of the Thomas-Fermi theory consisting in including additional terms to the energy depending on derivatives of the nucleon distributions, either phenomenological or as corrections arising from a semiclassical expansion, have been shown to play an important role. For instance, no pasta was found at the Thomas-Fermi level using the SLy4 nuclear parametrization [17] consistently with liquid-drop predictions [16] whereas pastas emerged when corrections were added [14, 19]. The results may also depend on the numerical implementation, and in particular on the parametrization of the nucleon distributions [20, 21].

Although the Thomas-Fermi theory and the generalizations discussed above are more realistic than liquid-drop models, they remain semiclassical and therefore they do not account for some quantum features such as shell effects or pairing. These corrections are of particular importance for determining the equilibrium composition, and more specifically the number of protons bound inside clusters, which in turn enters into the calculations of transport properties. On the other hand, fully microscopic three-dimensional calculations based on self-consistent (nonrelativistic and relativistic) mean-field models remain computationally very costly and for this reason have been so far carried out over a limited set of densities for fixed proton fractions and/or cell sizes [20, 22–25]. The main challenge is the proper description of continuum states within the classical band theory of solids, which requires the implementation of Floquet-Bloch boundary conditions (see the discussions in Refs. [26–28]). Neutron band states in neutron stars were first studied in Ref. [29] based on the known solutions of the 1D Kronig-Penney potential. The first detailed band-structure calculations for the different nuclear shapes using realistic mean fields were performed in Refs. [30, 31]. Most often, the mean-field equations are solved with strictly periodic boundary conditions instead. This leads to spurious shell effects [26, 32], which may introduce some uncontrolled bias in the search for the equilibrium shapes. To circumvent these difficulties, over the past years we have developed a computationally much faster approximation consisting in adding quantum

corrections perturbatively and, more importantly, consistently on top of the energy calculated semiclassically [33–36].

We have recently adapted this approach to investigate the existence of nuclear pastas in neutron stars [21, 37]. After reviewing our model in section 2, new results will be presented and discussed in section 3.

2 Extended Thomas-Fermi approach with quantum corrections

The extended Thomas-Fermi (ETF) method, which was originally developed to describe atomic nuclei in vacuum [38], is based on a systematic expansion of the smooth part of the single-particle quantum density of states in powers of $\hbar$. In this way, the energy of the nucleus becomes a functional of the local nucleon number densities $n_q(\boldsymbol{r})$ ($q = n, p$ for neutrons, protons respectively) at position $\boldsymbol{r}$ and their derivatives. The lowest order is the Thomas-Fermi theory. In application to neutron-star crusts, it is sufficient to calculate the energy of a single Wigner-Seitz cell. Full details can be found in Refs. [21, 33–37]. For simplicity, we consider three different types of cells, namely spherical, cylindrical and plate like corresponding to gnocchis/Swiss cheese, spaghetti/bucatini, and lasagna respectively. We include corrections up to the fourth order and we consider zero-range effective nucleon-nucleon interactions of the Skyrme type allowing for density-dependent generalizations of the t_1 and t_2 terms [39]. To further reduce the computational time, we parametrize the nucleon number densities as follows:

$$n_q(\xi) = n_{Bq} + n_{\Lambda q} f_q(\xi) \quad , \tag{1}$$

in which

$$f_q(\xi) = \frac{1}{1 + \exp\left[\left(\frac{C_q - R}{\xi - R}\right)^2 - 1\right] \exp\left(\frac{\xi - C_q}{a_q}\right)} \tag{2}$$

and ξ denotes the radial coordinate r in the case of spherical cells, the radial coordinate η in the case of cylindrical cells and z, the Cartesian coordinate for plates, assumed to lie in the $x - y$ plane. The parameter R likewise represents the radius of the spherical cell, the radius of the cylindrical cell or the semi-thickness of the plate-like cell. The parameter C_q represents the characteristic size of the cluster, as defined here by the half-width at half maximum of the nucleon distribution after removing the background contribution n_{Bq}. The diffuseness of the surface is determined by the parameter a_q. Inverted configurations occur whenever the cluster density $n_{\Lambda q} < 0$. With this parametrization the gradients of the nucleon densities vanish at the cell edge thus ensuring a proper matching with the nucleon background. For each given mean baryon number density $\bar{n}$, the optimum nucleon distributions $\widetilde{n_q}(\boldsymbol{r})$ are found by minimizing the energy per nucleon (after subtracting out the neutron mass energy by convention) given by

$$e^{\mathrm{ETF}} = e_{\mathrm{nuc}} + e_{\mathrm{C}} + e_e - Y_p \, Q_{n,\beta} \quad , \tag{3}$$

where e_{nuc} is the purely nuclear contribution, e_{C} the Coulomb contribution, e_e is the kinetic energy per nucleon of a fully degenerate relativistic electron Fermi gas, Y_p is the proton fraction, and $Q_{n,\beta}$ denotes the beta-decay energy of the neutron. The nuclear part is calculated by integrating inside the Wigner-Seitz cell the energy density given by Eq. (A3) of Ref. [39] using the ETF expressions for the kinetic-energy densities $\tau_q(\boldsymbol{r})$ and spin-current densities $\boldsymbol{J}_q(\boldsymbol{r})$ (see, e. g., Ref. [40]).

In a second stage, corrections are added to the ETF energy e^{ETF} to account for shell effects and pairing via the Strutinsky-integral method (SI). As argued in Ref. [37], the corrections for neutrons are expected to be much smaller than for protons and are therefore neglected. The

equilibrium configuration is then determined by searching for the lowest value of the total energy per nucleon given by

$$e = e^{\mathrm{ETF}} + \frac{1}{A}\left(E_p^{\mathrm{SI,pair}} + E_p^{\mathrm{pair}}\right) \quad , \tag{4}$$

where $E_p^{\mathrm{SI,pair}}$ is the SI correction for protons modified by pairing, E_p^{pair} is the proton pairing energy, and A is the number of nucleons in the Wigner-Seitz cell. These corrections are calculated by solving the Hartree-Fock (HF) equation

$$\left\{-\boldsymbol{\nabla}\frac{\hbar^2}{2\widetilde{M_p^*}(\boldsymbol{r})}\cdot\boldsymbol{\nabla} + \widetilde{U_p}(\boldsymbol{r}) + \widetilde{U_{\mathrm{C}}}(\boldsymbol{r}) - i\widetilde{\boldsymbol{W_p}}(\boldsymbol{r})\cdot\boldsymbol{\nabla}\times\boldsymbol{\sigma}\right\}\psi_{\nu,p} = \widetilde{\epsilon}_{\nu,p}\psi_{\nu,p} \quad , \tag{5}$$

where $\psi_{\nu,p}(\boldsymbol{r})$ is the proton wave function associated with the quantum state ν and $\widetilde{\epsilon}_{\nu,p}$ the associated single-particle energy. Here $\boldsymbol{\sigma}$ denotes the Pauli spin matrices. The proton effective mass $\widetilde{M_p^*}(\boldsymbol{r})$, the proton scalar potential $\widetilde{U_p}(\boldsymbol{r})$ and the proton spin-orbit vector potential $\widetilde{\boldsymbol{W_p}}(\boldsymbol{r})$ are calculated from Eqs. (A10), (A11) and (A12) of Ref. [39] respectively using the smooth ETF nucleon densities $\widetilde{n_q}(\boldsymbol{r})$ and corresponding ETF kinetic densities $\widetilde{\tau}_q(\boldsymbol{r})$ and spin current densities $\widetilde{\boldsymbol{J_q}}(\boldsymbol{r})$. The Coulomb potential $\widetilde{U_{\mathrm{C}}}(\boldsymbol{r})$ is obtained from the solution of Poisson's equation inside the Wigner-Seitz cell. Pairing is treated within the Bardeen-Cooper-Schrieffer (BCS) theory. The corrections then read [35]

$$E_p^{\mathrm{SI,pair}} = \sum_\nu V_{\nu,p}^2\,\widetilde{\epsilon}_{\nu,p} - \int d^3\boldsymbol{r}\left\{\frac{\hbar^2}{2\widetilde{M_p^*}(\boldsymbol{r})}\widetilde{\tau}_p(\boldsymbol{r}) + \widetilde{n_p}(\boldsymbol{r})\left[\widetilde{U_p}(\boldsymbol{r}) + \widetilde{U_{\mathrm{C}}}(\boldsymbol{r})\right] + \widetilde{\boldsymbol{J_p}}(\boldsymbol{r})\cdot\widetilde{\boldsymbol{W_p}}(\boldsymbol{r})\right\} \quad , \tag{6}$$

$$E_p^{\mathrm{pair}} = -\frac{1}{4}\sum_\nu \frac{\Delta_{\nu,p}^2}{E_{\nu,p}} \quad , \tag{7}$$

where $E_{\nu,p} = \sqrt{\left(\widetilde{\epsilon}_{\nu,p} - \mu_p\right)^2 + \Delta_{\nu,p}^2}$ is the quasiparticle energy, $\Delta_{\nu,p}$ is the BCS pairing gap, $V_{\nu,p}$ is the BCS occupation factor given by

$$V_{\nu,p} = \frac{1}{2}\left(1 - \frac{\widetilde{\epsilon}_{\nu,p} - \mu_p}{E_{\nu,p}}\right) \quad , \tag{8}$$

and the proton chemical potential μ_p is fixed by the condition (Z being the number of protons in the Wigner-Seitz cell)

$$\sum_\nu V_{\nu,p}^2 = Z \quad . \tag{9}$$

This so called ETFSI method was shown to yield results in good agreement with those obtained from solutions of the original mean-field equations, when using the same numerical setup [41]. This method amounts to iterating only once the HF equations using from the smooth ETF fields whereas the BCS gap equations are solved without any further approximation. Systematic calculations in all layers of the inner crust of a neutron star but restricted to spherical configurations can be found in Ref. [36], where consistent results for the outer crust and core using the same nuclear parametrizations were also presented.

For the region of interest where pasta phases are expected to occur, further simplifications are introduced, as discussed in Refs. [21, 37]. In particular, we evaluate the correction due to pairing by the associated condensation energy. The quantum corrections are thus written as $E_p^{\mathrm{SI,pair}} + E_p^{\mathrm{pair}} \approx E_p^{\mathrm{SI}} + E_p^{\mathrm{cond}}$, where E_p^{SI} is the SI correction in the absence of pairing and the proton condensation energy is given by

$$E_p^{\mathrm{cond}} = -\frac{3}{8}\int d^3\boldsymbol{r}\, n_p(\boldsymbol{r})\frac{\Delta_p(\boldsymbol{r})^2}{\epsilon_F(\boldsymbol{r})} \quad . \tag{10}$$

Here $\Delta_p(\boldsymbol{r})$ is the proton pairing gap of homogeneous nuclear matter of the appropriate density and charge asymmetry. Also, $\epsilon_F(\boldsymbol{r})$ is the local Fermi energy,

$$\epsilon_F(\boldsymbol{r}) = \frac{\hbar^2}{2M_p}\left(3\pi^2 n_p(\boldsymbol{r})\right)^{2/3} \quad . \tag{11}$$

The spin-orbit coupling in Eq. (5) is very small and is therefore neglected. The first term in Eq. (6) involves integrations over wavevectors associated with longitudinal motions. To avoid great complications, the proton effective mass is absorbed into the proton potential since integrations can then be performed analytically (see Ref. [37] for the expression of $E_p^{\rm SI}$). For consistency, spherical configurations are treated using the same approximations. The onset of proton drip is determined as discussed in Ref. [37].

3 Results and discussion

For numerical applications, we adopt the nuclear parametrization BSk24 [42], which was precision fitted to a large set of experimental nuclear data (including binding energies and charge radii) as well as theoretical data from ab initio calculations in infinite homogeneous nuclear matter (including the equation of state, effective masses, and ^{1}S$_0$ pairing gaps). This parametrization was previously employed in Refs. [21, 36, 37, 43] to calculate the internal constitution of neutron stars, their equation of state as well as their superfluid properties and was shown to be consistent with current astrophysical observations including those from the LIGO-Virgo collaboration on the gravitational-wave signal GW170817 as well as those from NICER [44, 45]. We have written a new Python code applying the SciPy library for the minimization procedure to improve the calculations, especially in the deepest regions of the crust near the boundary with the core where our previous code failed to converge for some densities.

To better assess the role of quantum effects on nuclear pastas, we have performed two sets of calculations by determining the equilibrium configuration with and without the quantum corrections. Our results are displayed in figure 1. Compared to our previously published calculations [21, 37], we now find that lasagna are no longer present and are replaced by bucatini, both in the ETF and ETFSI treatments. However, our main conclusion that pastas almost completely vanish when the quantum corrections are taken into account still holds. More specifically, the mass fraction of the pasta phases falls from $\sim 48\%$ to only $\sim 4\%$.

Our results are at variance with those recently obtained from mean-field calculations [25]. This discrepancy might be due to the approximations we made within the ETFSI approach and/or the implementation of the mean-field equations in Ref. [25]. In particular, although the parametrization NRAPR [46] employed in Ref. [25] was constrained to reproduce realistic calculations in infinite homogeneous nuclear matter, it was only fitted to the charge radii and the binding energies of just three even-even magic nuclei (two of which being also doubly magic), namely ^{208}Pb, ^{90}Zr, and ^{40}Ca while 2353 nuclei of all kinds were included in the fit of BSk24 (in addition to nuclear-matter properties, as previously mentioned). Therefore the NRAPR parametrization does not seem to be very well suited for describing the very neutron-rich pasta region in neutron stars unlike the BSk24 parametrization that we have adopted for our ETFSI calculations. More importantly, the results of Ref. [25] are prone to systematic errors incurred by the use of periodic boundary conditions, as discussed by the authors themselves (see also the discussion in section 1). For this reason, they wrote that they were unable to determine the equilibrium cell size. Instead, they considered cell sizes around values predicted by a compressible liquid-drop model with the same parametrization NRAPR for the bulk part. Therefore, the configurations they found may not correspond to the true equilibrium state.

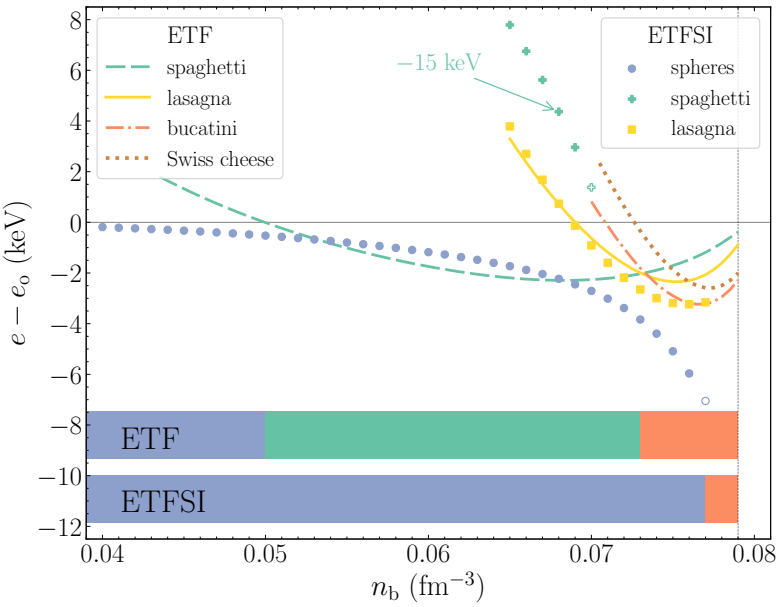

Figure 1. Energy per nucleon for different pasta phases with ETF energy of spheres subtracted versus baryon number density. Lines correspond to ETF calculations: green dashed for spaghetti, yellow solid for lasagna, orange dash-dotted for bucatini and dotted brown for Swiss cheese. ETFSI results are indicated by symbols: blue circles for spheres, green crosses for spaghetti and yellow squares for lasagna. Note that the ETFSI energies for spaghetti have been shifted by 15 keV to make them visible on the plot. Bars in the bottom part represent the different pasta regions with the same color coding.

4 Conclusions

The existence of nuclear pastas in neutron stars is found to be extremely sensitive to quantum effects. Whereas nuclear pastas represent a sizable fraction of the mass of the neutron-star crust at the ETF level in agreement with previous predictions from liquid-drop models [10–12], they almost completely vanish when shell and pairing corrections are included on top of the ETF energy (3). Quantum effects may thus play a more important role than previously thought. However, further studies are needed to confirm this conclusion considering other nuclear parametrizations consistent with our current knowledge of nuclear physics.

This work was financially supported by F.R.S.-FNRS (Belgium) under Grant No. IISN 4.4502.19. It has also received funding from the FWO (Belgium) and the F.R.S.-FNRS (Belgium) under the Excellence of Science (EOS) programme (project No. 40007501).

References

[1] B. Posselt, G.G. Pavlov, ApJ**932**, 83 (2022), 2205.06552
[2] D. Blaschke, N. Chamel, *Phases of Dense Matter in Compact Stars*, in *Astrophysics and Space Science Library*, edited by L. Rezzolla, P. Pizzochero, D.I. Jones, N. Rea, I. Vidaña (2018), Vol. 457 of *Astrophysics and Space Science Library*, p. 337
[3] N. Chamel, A.F. Fantina, Phys. Rev. C**94**, 065802 (2016), 2103.06073
[4] G. Baym, H.A. Bethe, C.J. Pethick, Nucl. Phys. A**175**, 225 (1971)

[5] D.G. Ravenhall, C.J. Pethick, J.R. Wilson, Phys. Rev. Lett.**50**, 2066 (1983)
[6] M. Hashimoto, H. Seki, M. Yamada, Progress of Theoretical Physics **71**, 320 (1984)
[7] K. Oyamatsu, M. Hashimoto, M. Yamada, Progress of Theoretical Physics **72**, 373 (1984)
[8] S. Kubis, W. Wójcik, Physics Letters B **835**, 137474 (2022), 2102.06675
[9] N.A. Zemlyakov, A.I. Chugunov, Particles **5**, 225 (2022), 2209.05851
[10] C.P. Lorenz, D.G. Ravenhall, C.J. Pethick, Phys. Rev. Lett.**70**, 379 (1993)
[11] H. Dinh Thi, T. Carreau, A.F. Fantina, F. Gulminelli, A&A**654**, A114 (2021), 2109.13638
[12] W.G. Newton, R. Preston, L. Balliet, M. Ross, Physics Letters B **834**, 137481 (2022), 2111.07969
[13] N.A. Zemlyakov, A.I. Chugunov, N.N. Shchechilin, *Non-spherical nucleon clusters in the mantle of a neutron star: CLDM based on Skyrme-type forces*, in *Journal of Physics Conference Series* (2021), Vol. 2103 of *Journal of Physics Conference Series*, p. 012004
[14] N.N. Shchechilin, N.A. Zemlyakov, A.I. Chugunov, M.E. Gusakov, Universe **8** (2022)
[15] F. Douchin, P. Haensel, J. Meyer, Nucl. Phys. A**665**, 419 (2000)
[16] X. Viñas, C. Gonzalez-Boquera, B.K. Sharma, M. Centelles, Acta Physica Polonica B, Proceedings Supplement **10**, 259 (2017)
[17] E. Chabanat, P. Bonche, P. Haensel, J. Meyer, R. Schaeffer, Nucl. Phys. A**635**, 231 (1998)
[18] Y. Lim, J.W. Holt, Phys. Rev. C**95**, 065805 (2017)
[19] N. Martin, M. Urban, Phys. Rev. C**92**, 015803 (2015), 1505.07030
[20] P. Gögelein, H. Müther, Phys. Rev. C**76**, 024312 (2007), 0704.1984
[21] J.M. Pearson, N. Chamel, A.Y. Potekhin, Phys. Rev. C**101**, 015802 (2020), 2001.03876
[22] P. Magierski, P.H. Heenen, Phys. Rev. C**65**, 045804 (2002), nucl-th/0112018
[23] F.J. Fattoyev, C.J. Horowitz, B. Schuetrumpf, Phys. Rev. C**95**, 055804 (2017), 1703.01433
[24] B. Schuetrumpf, G. Martínez-Pinedo, M. Afibuzzaman, H.M. Aktulga, Phys. Rev. C**100**, 045806 (2019), 1906.08155
[25] W.G. Newton, S. Cantu, S. Wang, A. Stinson, M.A. Kaltenborn, J.R. Stone, Phys. Rev. C**105**, 025806 (2022), 2104.11835
[26] N. Chamel, S. Naimi, E. Khan, J. Margueron, Phys. Rev. C**75**, 055806 (2007), astro-ph/0701851
[27] N. Chamel, Phys. Rev. C**85**, 035801 (2012)
[28] B. Schuetrumpf, W. Nazarewicz, Phys. Rev. C**92**, 045806 (2015), 1508.06611
[29] K. Oyamatsu, M. Yamada, Nucl. Phys. A**578**, 181 (1994)
[30] B. Carter, N. Chamel, P. Haensel, Nucl. Phys. A**748**, 675 (2005), nucl-th/0402057
[31] N. Chamel, Nucl. Phys. A**747**, 109 (2005), nucl-th/0405003
[32] W.G. Newton, J.R. Stone, Phys. Rev. C**79**, 055801 (2009)
[33] M. Onsi, A.K. Dutta, H. Chatri, S. Goriely, N. Chamel, J.M. Pearson, Phys. Rev. C**77**, 065805 (2008), 0806.0296
[34] J.M. Pearson, N. Chamel, S. Goriely, C. Ducoin, Phys. Rev. C**85**, 065803 (2012), 1206.0205
[35] J.M. Pearson, N. Chamel, A. Pastore, S. Goriely, Phys. Rev. C**91**, 018801 (2015)
[36] J.M. Pearson, N. Chamel, A.Y. Potekhin, A.F. Fantina, C. Ducoin, A.K. Dutta, S. Goriely, MNRAS**481**, 2994 (2018), 1903.04981

[37] J.M. Pearson, N. Chamel, Phys. Rev. C**105**, 015803 (2022)
[38] M. Brack, C. Guet, H.B. Håkansson, Phys. Rep.**123**, 275 (1985)
[39] N. Chamel, S. Goriely, J.M. Pearson, Phys. Rev. C**80**, 065804 (2009), 0911.3346
[40] M. Onsi, H. Przysiezniak, J.M. Pearson, Phys. Rev. C**55**, 3139 (1997)
[41] M. Shelley, A. Pastore, Universe **6**, 206 (2020), 2011.10511
[42] S. Goriely, N. Chamel, J.M. Pearson, Phys. Rev. C**88**, 061302 (2013)
[43] V. Allard, N. Chamel, arXiv e-prints arXiv:2203.08778 (2022), 2203.08778
[44] L. Perot, N. Chamel, A. Sourie, Phys. Rev. C**100**, 035801 (2019), 1910.13202
[45] L. Perot, N. Chamel, arXiv e-prints arXiv:2203.09145 (2022), 2203.09145
[46] A.W. Steiner, M. Prakash, J.M. Lattimer, P.J. Ellis, Phys. Rep.**411**, 325 (2005), nucl-th/0410066